nature biotechnology

ARTICLES

https://doi.org/10.1038/s41587-021-00982-9



# RNA demethylation increases the yield and biomass of rice and potato plants in field trials

Qiong Yu[1,10], Shun Liu[2,3,10], Lu Yu[4], Yu Xiao[1], Shasha Zhang[1], Xueping Wang[1], Yingying Xu[1], Hong Yu[5], Yulong Li[6], Junbo Yang[1], Jun Tang[1], Hong-Chao Duan[1], Lian-Huan Wei[1], Haiyan Zhang[7], Jiangbo Wei[2,3], Qian Tang[1], Chunling Wang[1], Wutong Zhang[1], Ye Wang[1], Peizhe Song[1], Qiang Lu[1], Wei Zhang[1], Shunqing Dong[1], Baoan Song[4] ✉, Chuan He[2,3,8] ✉ and Guifang Jia[1,9] ✉

**RNA $N^6$-methyladenosine ($m^6A$) modifications are essential in plants. Here, we show that transgenic expression of the human RNA demethylase FTO in rice caused a more than threefold increase in grain yield under greenhouse conditions. In field trials, transgenic expression of FTO in rice and potato caused ~50% increases in yield and biomass. We demonstrate that the presence of FTO stimulates root meristem cell proliferation and tiller bud formation and promotes photosynthetic efficiency and drought tolerance but has no effect on mature cell size, shoot meristem cell proliferation, root diameter, plant height or ploidy. FTO mediates substantial $m^6A$ demethylation (around 7% of demethylation in poly(A) RNA and around 35% decrease of $m^6A$ in non-ribosomal nuclear RNA) in plant RNA, inducing chromatin openness and transcriptional activation. Therefore, modulation of plant RNA $m^6A$ methylation is a promising strategy to dramatically improve plant growth and crop yield.**

To meet the increasing food demand caused by population growth, numerous strategies have to be attempted to increase plant production[1]. More than 30 years of transgenic research have led to notable advances in engineering crops for higher yield through transformation of exogenous and endogenous genes[2], for example, by introduction of insect resistance with bacterial toxins[3], herbicide tolerance with bacterial enzymes degrading herbicides[4] and engineering disease resistance with endogenous genes[5]. Multiple endogenous genes have also been manipulated to directly increase yields by engineering plant architecture, nitrogen use and other pathways[6–8]. Modulation of photorespiratory pathways to enhance $C_3$ crop photosynthetic efficiency is another modern strategy to increase yield via engineering of plant glycolate metabolism with bacterial genes[9]. The emerging field of epitranscriptomics has revealed extensive post-transcriptional regulation of RNA metabolism affecting cell differentiation and development[10], but whether the epitranscriptome can be engineered to stimulate crop production remains unexplored.

$m^6A$ is the most abundant mRNA modification in higher eukaryotes; it can be dynamically written, read and erased to regulate RNA processing and metabolism[11,12]. In mammalian systems, the $m^6A$ methylation mark is essential: knockout of the gene encoding METTL3 $m^6A$ methyltransferase is embryonic lethal in mice[13]. Human FTO, originally identified as a fat mass- and obesity-associated protein[14], mediates RNA $m^6A$ demethylation[15]. Different RNA modifications can be demethylated by FTO in human cells, including $m^6A$ in poly(A) RNA and U6 small nuclear RNA (snRNA), $N^6$,2′-$O$-dimethyladenosine ($m^6A_m$) at the cap +1 position in poly(A) RNA, cap and internal $m^6A_m$ in U1 and U2 snRNA and $N^1$-methyladenosine ($m^1A$) in tRNA[15–18]. FTO-mediated $m^6A$ demethylation was shown to affect cell growth and proliferation[19]. In plants, $m^6A$ is also required for normal development: early works showed that disruption of an $m^6A$ writer subunit leads to embryonic lethality in *Arabidopsis*[20–23] and early degeneration of microspores in rice[24]; that plant RNA $m^6A$ demethylases ALKBH10B and ALKBH9B, homologs of the human $m^6A$ demethylase ALKBH5 (ref. [25]), affect floral transition[26] and viral infection[27]; and that plant $m^6A$ reader proteins appear to affect multiple physiological properties in *Arabidopsis*[28–34]. As these results all indicate that $m^6A$ does affect plant growth and physiology, we speculated that manipulation of plant $m^6A$ levels via introduction of an $m^6A$ demethylase might offer a new means to affect plant growth.

Because plants do not have an FTO homolog, we pursued this idea about potential growth-altering effects of manipulating the plant epitranscriptome by introducing human FTO. We envisioned that, as a 'foreign' protein, FTO may not be recognized or controlled by plant components. Its demethylation activity may affect multiple potential targets to yield unexpected effects. Here we report that transgenic expression of FTO increases rice and potato yields and biomass by ~50% in field trials. Expression of FTO enhances root growth, tiller bud formation, photosynthetic efficiency and drought tolerance. FTO specifically promotes root meristem cell proliferation, leading to larger root numbers and length. All these phenotypes require the demethylation activity of FTO. We further demonstrated that FTO-mediated $m^6A$ demethylation promotes chromatin openness and induces transcriptional activation. Our

[1]Synthetic and Functional Biomolecules Center, Beijing National Laboratory for Molecular Sciences, Key Laboratory of Bioorganic Chemistry and Molecular Engineering of Ministry of Education, College of Chemistry and Molecular Engineering, Peking University, Beijing, China. [2]Department of Chemistry and Institute for Biophysical Dynamics, The University of Chicago, Chicago, IL, USA. [3]Howard Hughes Medical Institute, Chicago, IL, USA. [4]State Key Laboratory Breeding Base of Green Pesticide and Agricultural Bioengineering/Key Laboratory of Green Pesticide and Agricultural Bioengineering, Ministry of Education, Guizhou University, Guiyang, China. [5]State Key Laboratory of Plant Genomics, Institute of Genetics and Developmental Biology, The Innovative Academy of Seed Design, Chinese Academy of Sciences, Beijing, China. [6]School of Life Sciences, Jiangsu University, Zhenjiang, China. [7]College of Life Sciences, Tianjin Normal University, Tianjin, China. [8]Department of Biochemistry and Molecular Biology, The University of Chicago, Chicago, IL, USA. [9]National Engineering Research Center of Pesticide, Nankai University, Tianjin, China. [10]These authors contributed equally: Qiong Yu, Shun Liu. ✉e-mail: songbaoan22@yahoo.com; chuanhe@uchicago.edu; guifangjia@pku.edu.cn

study reveals that RNA m$^6$A modification is critical to control plant growth, and its modulation provides a new, promising approach to substantially elevate crop production.

## Results

**Active *FTO* transgene increases crop yield and biomass.** We generated transgenic rice plants expressing FTO in two genetic backgrounds, Nipponbare (Nipp) and Zhonghua11 (ZH11), as well as transgenic Nipp plants expressing a demethylation activity-dead mutant variant of FTO (FTO$^{R316Q/R322Q}$, designated *FTO*$^{mut}$ rice) (Supplementary Fig. 1a,b). After confirming expression of FTO in plants of *FTO-1*, *FTO-2* (Nipp background) and *FTO-3* (ZH11 background) transgenic lines and expression of FTO$^{R316Q/R322Q}$ in *FTO*$^{mut}$ transgenic rice plants (Nipp background) (Supplementary Fig. 1c,d and Supplementary Tables 1 and 2), we characterized agronomic traits in the greenhouse (Supplementary Fig. 2a–d). To our surprise, the expression of *FTO* led to a more than threefold increase in grain yield and a more than twofold increase in aerial biomass (that is, above-ground matter, excluding grain) compared with those of wild-type (WT) control rice under greenhouse conditions (Supplementary Fig. 2d). We subsequently conducted field trials with homozygous transgenic and WT plants at two different locations in China (Jiangxi and Beijing). Consistently, rice expressing catalytically active FTO showed significantly increased grain yield and biomass compared to both WT and inactive *FTO*$^{mut}$ plants in the field (Fig. 1a,b).

Specifically, all three transgenic rice lines expressing catalytically active FTO showed over 47% higher grain yield and grain number and over 40% higher biomass in the field (Fig. 1c,d and Supplementary Fig. 3a). Moreover, examination of plants in the field before the heading stage showed that *FTO*-transgenic rice exhibited a more than 42% increase in the number of total tillers as well as total productive tillers per plant (that is, tillers that ultimately produce a grain-bearing panicle) compared with WT or *FTO*$^{mut}$ rice (Fig. 1e and Supplementary Fig. 3b); almost all of the increased tillers in *FTO* rice plants eventually developed into productive tillers. Further evaluation of the various phenotypes in this field study revealed no significant differences in grain size, thousand-grain weight, main panicle grain number, major spike length, mature plant height or heading time (Supplementary Fig. 3c–h), suggesting that the observed higher grain yield and aerial biomass in *FTO*-transgenic rice result primarily from the substantial increase in the productive tiller number. Thus, the RNA demethylation activity of FTO can confer massive increases in multiple economically impactful agronomic traits in the globally essential monocot cereal crop rice. These growth phenotypes are dependent on the demethylation activity of FTO, as *FTO*$^{mut}$ plants expressing catalytically inactive FTO did not exhibit these traits.

The growth promotion effect was not limited to monocot rice. When we transgenically expressed FTO in the eudicot tuber crop potato (*Solanum tuberosum*, Emalingshu3 (EM3) background) (Supplementary Fig. 1c,d and Supplementary Tables 3 and 4), we observed similarly massive increases in both yield and aerial biomass (Fig. 1f–h). We found that, although FTO did not cause potato plants to produce significantly more tubers (Fig. 1i), it led to ~50% increases in yield (assessed as total tuber weight) and aerial biomass (Fig. 1g,h). Thus, transgenic introduction of *FTO* can confer drastic yield and biomass increases in dicotyledonous plants.

We further investigated whether the *FTO* expression level and/or inheritance of the *FTO* transgene across generations may affect the high yield and biomass agronomic traits of rice plants. After testing the field phenotypes of four *FTO*-transgenic rice lines (Nipp background) with varied *FTO* expression levels and three generations ($T_2$ to $T_4$) of the *FTO-1* lines, we found that all these plants exhibited the aforementioned phenotypes, including more than a 40% increase in grain yield (Supplementary Fig. 4a,b). More discussion is provided in the Supplementary Results. We also evaluated protein and amylose contents in *FTO*-transgenic rice grains and carbohydrate, starch, vitamin C and overall protein contents in *FTO*-transgenic potato tubers and found that expression of FTO did not alter these nutrition-related traits in rice grains or potato tubers as compared to those in the corresponding WT or *FTO*$^{mut}$ plants (Supplementary Fig. 5a–f).

**Active *FTO* transgene promotes root growth.** Seeking to further characterize the physiological impacts of introducing FTO, we examined 15-d-old seedlings and 2-month-old plants at the tillering stage of WT (Nipp), *FTO*$^{mut}$- and *FTO*-transgenic rice. We found that fresh weights of whole plants, aerial tissues and roots were all markedly increased at tillering and seedling stages of *FTO*-transgenic rice (Fig. 2a and Supplementary Figs. 6 and 7). Detailed evaluation of root morphological parameters at both stages using WinRHIZO software (Regent Instruments) revealed that roots offered the most visually striking difference for *FTO*-transgenic rice at the tillering stage (Supplementary Figs. 8 and 9 and Methods). Compared to WT seedlings, *FTO* rice seedlings showed around 33% and 45% increases in the total root number and the total length of lateral roots (Supplementary Fig. 8b,g). We also noted that *FTO* rice plants exhibited more than a 3.3-fold increase in both number and length of primary roots (4.4-fold and 3.3-fold increases in number and length, respectively) at the tillering stage when compared with WT plants (Supplementary Fig. 9b,e). Similar increases were also detected for lateral roots (3.7-fold increase in both number and length) (Supplementary Fig. 9c,f). There was no obvious differences in root diameter between *FTO* and WT plants at either the seedling (Supplementary Fig. 8h,i) or the tillering stage (Supplementary Fig. 9g,h). Note that we also compared WT and *FTO*$^{mut}$ plants in these analyses and found no phenotypic differences.

**Active *FTO* transgene enhances root cell proliferation.** To characterize phenotypic differences in roots at the histological level and to seek clues about altered plant development programs, we examined cell size in root zones and mature leaves. Staining of longitudinal tissue sections of rice and potato plants showed that cell sizes in both root zones and mature leaves of *FTO* rice and potato plants did not differ from those of the corresponding WT or *FTO*$^{mut}$ plants (Supplementary Fig. 10a,b). These observations suggest that increases in root growth are likely caused by cell division, not cell elongation. Subsequently, we used confocal microscopy to examine meristem cells in propidium iodide (PI)-stained root tips. The size of *FTO* rice root apical meristem zones did not differ from that of WT or *FTO*$^{mut}$ roots; however, meristem cells of *FTO* roots had lesser longitudinal length and had higher overall meristem cell numbers (Fig. 2b), indicating that FTO expression in rice increases root apical meristem cell proliferation.

We also examined the shoot apical meristem and observed that shoot apical meristem size and numbers of the first layer of meristem cells were not altered among WT, *FTO* and *FTO*$^{mut}$ rice (Supplementary Fig. 11), consistent with our findings that *FTO*-transgenic rice did not differ in rice leaf size or plant height. To further confirm that FTO does increase root cell proliferation, we labeled newly replicated DNA using 5-ethynyl-2′-deoxyuridine (EdU) and found that the EdU signal was significantly increased in *FTO* rice roots compared with those of WT and *FTO*$^{mut}$ plants (Fig. 2c and Methods), supporting the notion that root cell division rate was increased by FTO. Collectively, these results reveal that expression of FTO in plants enhances root development by promoting cell division in the root meristem.

**Active *FTO* transgene promotes tiller bud formation.** Yields in cereal crops are strongly impacted by the number and type of tillers produced by individual plants[35]. We found that *FTO*-transgenic

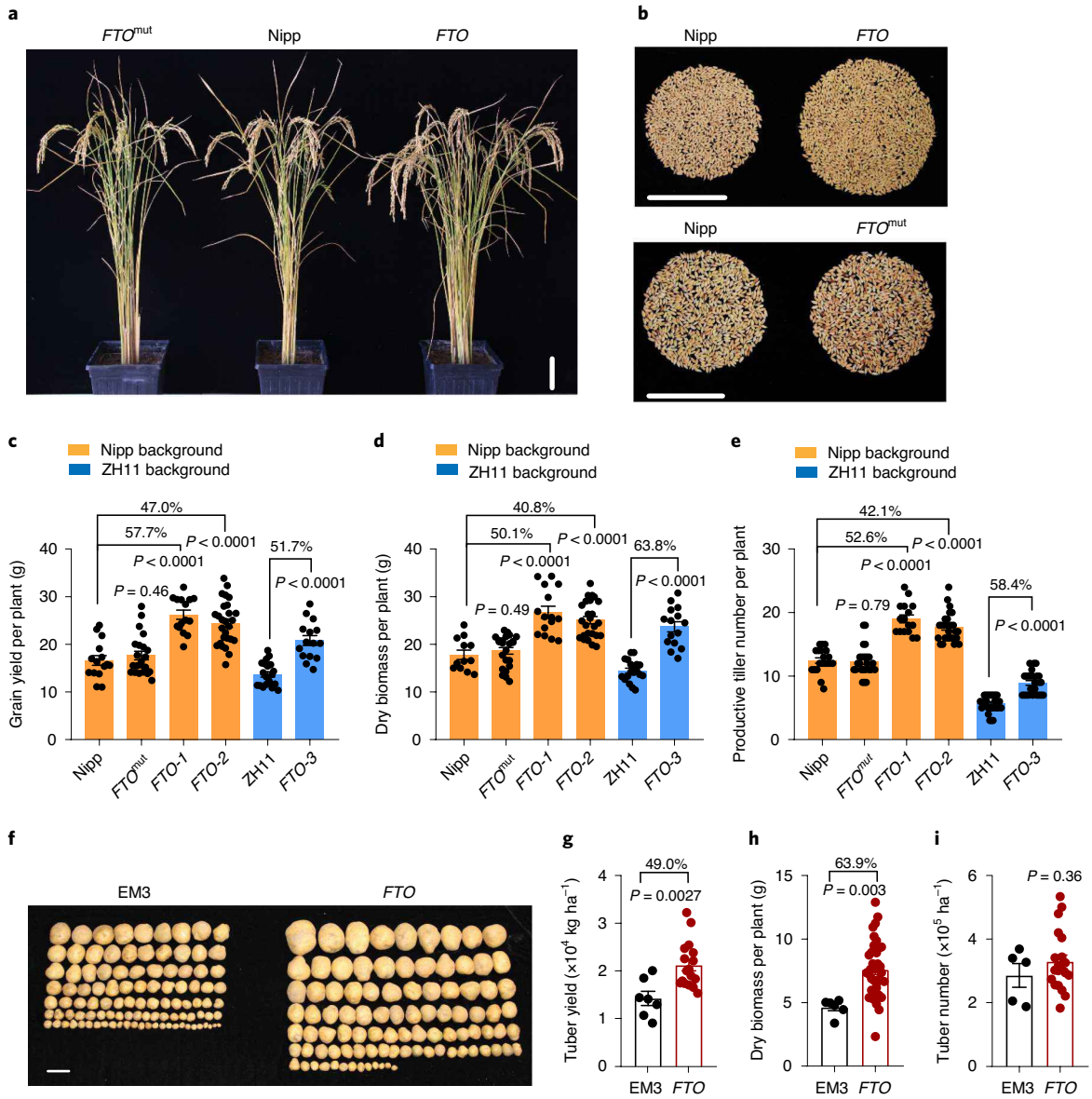


**Fig. 1 | Transgenic expression of FTO increases yield and biomass of rice and potato plants in the field. a**, Photos of mature WT (Nipp), *FTO* and *FTO*$^{mut}$ (a demethylation activity-dead mutant variant of FTO) rice plants grown in the field. Scale bar, 10 cm. **b**, Total grains per plant in WT (Nipp), *FTO*$^{mut}$- and *FTO*-transgenic rice plants in the field. Scale bars, 10 cm. **c**–**e**, Grain yield (**c**), dry biomass (**d**) and productive tiller number per plant (**e**) in the indicated rice lines grown in the field. Data are mean ± s.e.m. (**c**, $n = 15$ Nipp, $n = 22$ *FTO*$^{mut}$, $n = 15$ *FTO-1*, $n = 27$ *FTO-2*, $n = 20$ ZH11, $n = 15$ *FTO-3*; **d**, $n = 12$ Nipp, $n = 23$ *FTO*$^{mut}$, $n = 15$ *FTO-1*, $n = 25$ *FTO-2*, $n = 19$ ZH11, $n = 15$ *FTO-3*; **e**, $n = 20$ Nipp, $n = 25$ *FTO*$^{mut}$, $n = 16$ *FTO-1*, $n = 26$ *FTO-2*, $n = 27$ ZH11, $n = 24$ *FTO-3*). **f**, Photos of tubers harvested from 20 potato plants of WT (EM3) and *FTO*-transgenic backgrounds grown in the field. **g**,**i**, Tuber yield (**g**) and tuber number (**i**) in the indicated potato plants grown in the field. Data are mean ± s.e.m. of *n* plots (**g**, $n = 7$ EM3, $n = 17$ *FTO*; **i**, $n = 5$ EM3, $n = 20$ *FTO*; each plot contained over 50 plants). **h**, Dry biomass per plant of the indicated potato plants grown in the greenhouse. Data are mean ± s.e.m. ($n = 6$ EM3, $n = 36$ *FTO*). *P* values are from unpaired, two-tailed Student's *t*-tests.

rice had a greater than 40% increase in the number of productive tillers (Fig. 1e). Given that the development of productive tillers is controlled in a two-stage process including the formation of an axillary bud at the unelongated basal internode and the subsequent outgrowth of such buds[35], we next characterized the role of FTO in rice tillering ability at the anatomical level. *FTO*-transgenic rice as four-leaf-stage seedlings had significantly more axillary buds on the unelongated basal internode than WT and *FTO*$^{mut}$ plants at the same growth stage (Fig. 2d). Longitudinal sections further confirmed that 10-d-old *FTO*-transgenic rice had already formed a normal tiller bud but WT and *FTO*$^{mut}$ rice had not (Fig. 2e). Note that *FTO*-transgenic, WT and *FTO*$^{mut}$ plants did not have tillers on elongated upper internodes during field trials.

**FTO increases photosynthesis and drought tolerance.** Our observations of notable increases in diverse plant organs upon FTO expression suggest that this RNA-demethylase enzyme may affect multiple physiological processes in plants. Any increase in plant growth must be accompanied by increased carbon acquisition. Indeed, we found that FTO-expressing plants exhibited ~36% higher net photosynthetic efficiency than WT or *FTO*$^{mut}$ plants in the field (Fig. 2f). Consistently, *FTO*-transgenic plants

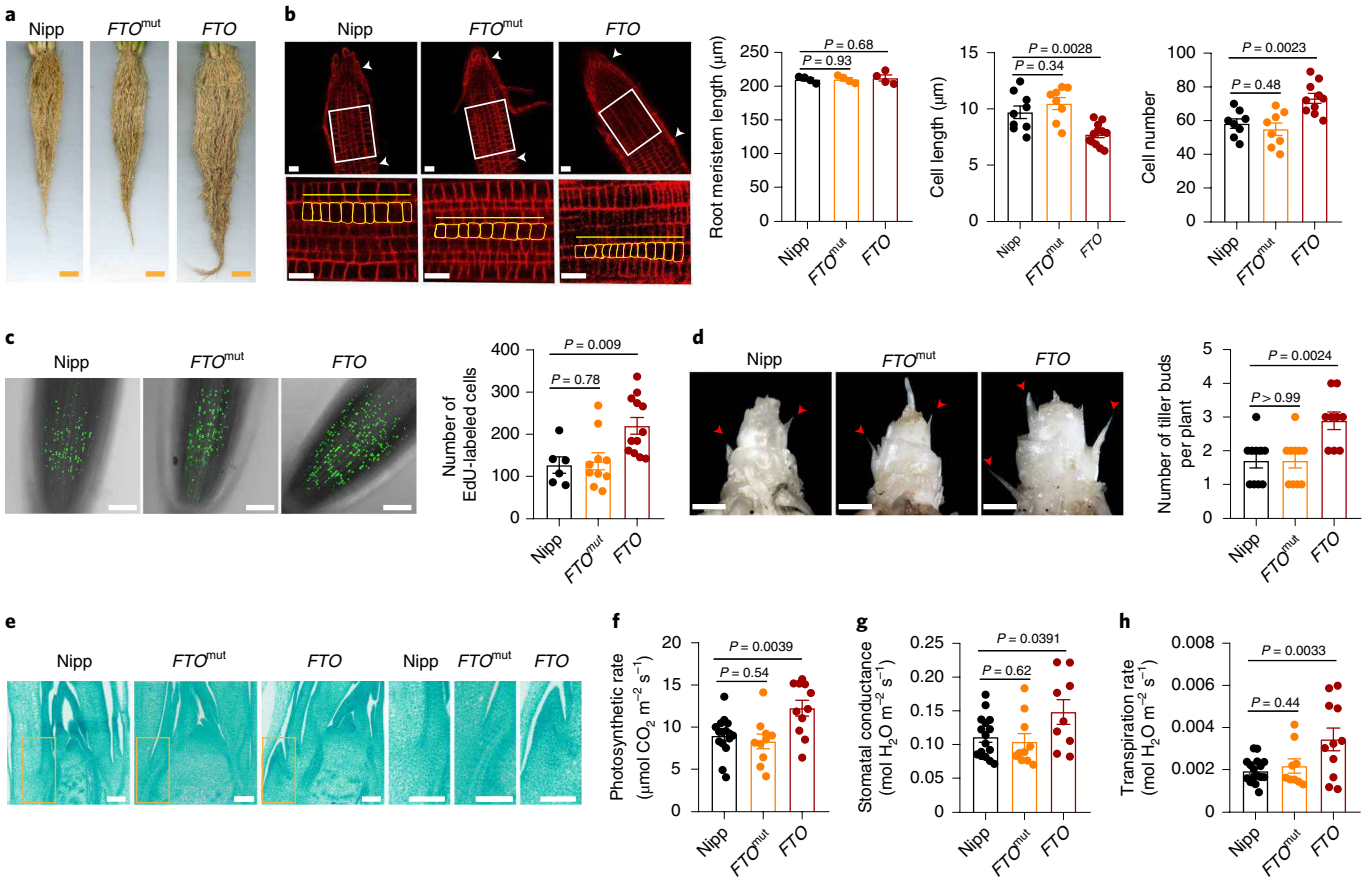


**Fig. 2 | FTO increases root meristem cell proliferation, root growth, tiller formation and photosynthesis efficiency. a**, Root photos of 2-month-old Nipp, *FTO*$^{mut}$- and *FTO*-transgenic rice at the tillering stage grown in the greenhouse. Scale bars, 2 cm. **b**, PI staining of root tips in 10-d-old Nipp, *FTO*$^{mut}$- and *FTO*-transgenic rice and quantitative analysis of root meristem length, cell length and cell number within the same length of the root meristem (as indicated in white boxes and magnified images at the bottom). Arrowheads indicate ends of root meristems. The cell length was calculated from the same length of the root meristem as indicated by the yellow line. Data are mean ± s.e.m. ($n = 4$ (left); $n = 9$ Nipp, $n = 8$ *FTO*$^{mut}$, $n = 12$ *FTO* (middle); $n = 8$ Nipp, $n = 8$ *FTO*$^{mut}$, $n = 10$ *FTO* (right)). Scale bars, 20 μm. **c**, Longitudinal view of EdU-labeled cells in root meristems of 4-d-old Nipp, *FTO*$^{mut}$- and *FTO*-transgenic rice seedlings. Scale bars, 20 μm. Numbers of EdU-labeled cells in root tips were counted. Data are mean ± s.e.m. ($n = 6$ Nipp, $n = 10$ *FTO*$^{mut}$, $n = 12$ *FTO*). **d**, Shoot basal regions of four-leaf stage Nipp, *FTO*$^{mut}$- and *FTO*-transgenic rice seedlings. Arrowheads indicate tiller buds. Scale bars, 1 mm. Data are mean ± s.e.m. ($n = 10$ Nipp, $n = 10$ *FTO*$^{mut}$, $n = 9$ *FTO*). **e**, Longitudinal sections of shoot apexes and tiller buds of 10-d-old Nipp, *FTO*$^{mut}$- and *FTO*-transgenic rice. Scale bars, 100 μm. The experiment was repeated three times independently with similar results. **f**–**h**, Photosynthetic rate (**f**), stomatal conductance (**g**) and transpiration rate (**h**) of Nipp, *FTO*$^{mut}$- and *FTO*-transgenic rice at the filling stage grown in a field in Beijing. Data are mean ± s.e.m. (**f**, $n = 16$ Nipp, $n = 10$ *FTO*$^{mut}$, $n = 11$ *FTO*; **g**, $n = 16$ Nipp, $n = 10$ *FTO*$^{mut}$, $n = 9$ *FTO*; **h**, $n = 17$ Nipp, $n = 9$ *FTO*$^{mut}$, $n = 11$ *FTO*). *P* values are from unpaired, two-tailed *t*-tests.

also showed a ~34% increase in stomata conductance and a ~78% increase in transpiration rates (Fig. 2g,h). Considering that stomatal opening might induce hypersensitivity in droughts[36], we tested whether *FTO* expression in rice affects drought resistance. Results showed that both 3- and 6-week-old *FTO* rice plants exhibited significantly higher survival rates under two drought stress treatment conditions compared to WT and *FTO*$^{mut}$ plants (Supplementary Fig. 12 and Supplementary Methods). Thus, these results show that *FTO*-transgenic plants possess enhanced photosynthetic efficiency and drought tolerance. More discussion on photosynthesis and drought tolerance is provided in the Supplementary Results.

**FTO mediates substantial nuclear m$^6$A demethylation.** To explore the potential molecular pathways through which FTO confers the observed phenotypes, we next investigated effects on RNA caused by expression of FTO. Both stably transformed *35S::FTO-eGFP* transgenic *Arabidopsis* root and tobacco leaves transformed with the *35S::FTO-eGFP* construct for transient expression showed that FTO is primarily localized in the nucleus (Supplementary Fig. 13), consistent with the main subcellular localization of FTO observed in mammals[15]. We examined how FTO affects m$^6$A levels in diverse organs of transgenic rice and potato plants. We isolated poly(A) RNA, non-ribosomal RNA and non-ribosomal nuclear RNA from different organs of WT, *FTO*$^{mut}$ and *FTO* plants and quantified the ratio of m$^6$A/A (a relative m$^6$A level) by liquid chromatography–tandem mass spectrometry (LC–MS/MS). Consistent with the known m$^6$A-demethylation function of FTO, samples from 15-d-old *FTO*-transgenic rice displayed noticeably reduced m$^6$A levels (reduction of around 7%) in poly(A) RNA isolated from both shoots and roots compared to those from WT and *FTO*$^{mut}$ plants. Notably, the non-ribosomal nuclear RNA portion showed a decrease of around 35% in m$^6$A level in *FTO*-transgenic rice seedlings compared to that from WT plants (Fig. 3a). FTO expression clearly caused more m$^6$A reduction in rice non-ribosomal nuclear RNA than that in rice total poly(A) RNA, which is consistent with the nuclear localization of overexpressed FTO in plants (Supplementary Fig. 13). This trend was evident for all tested organs at different stages and

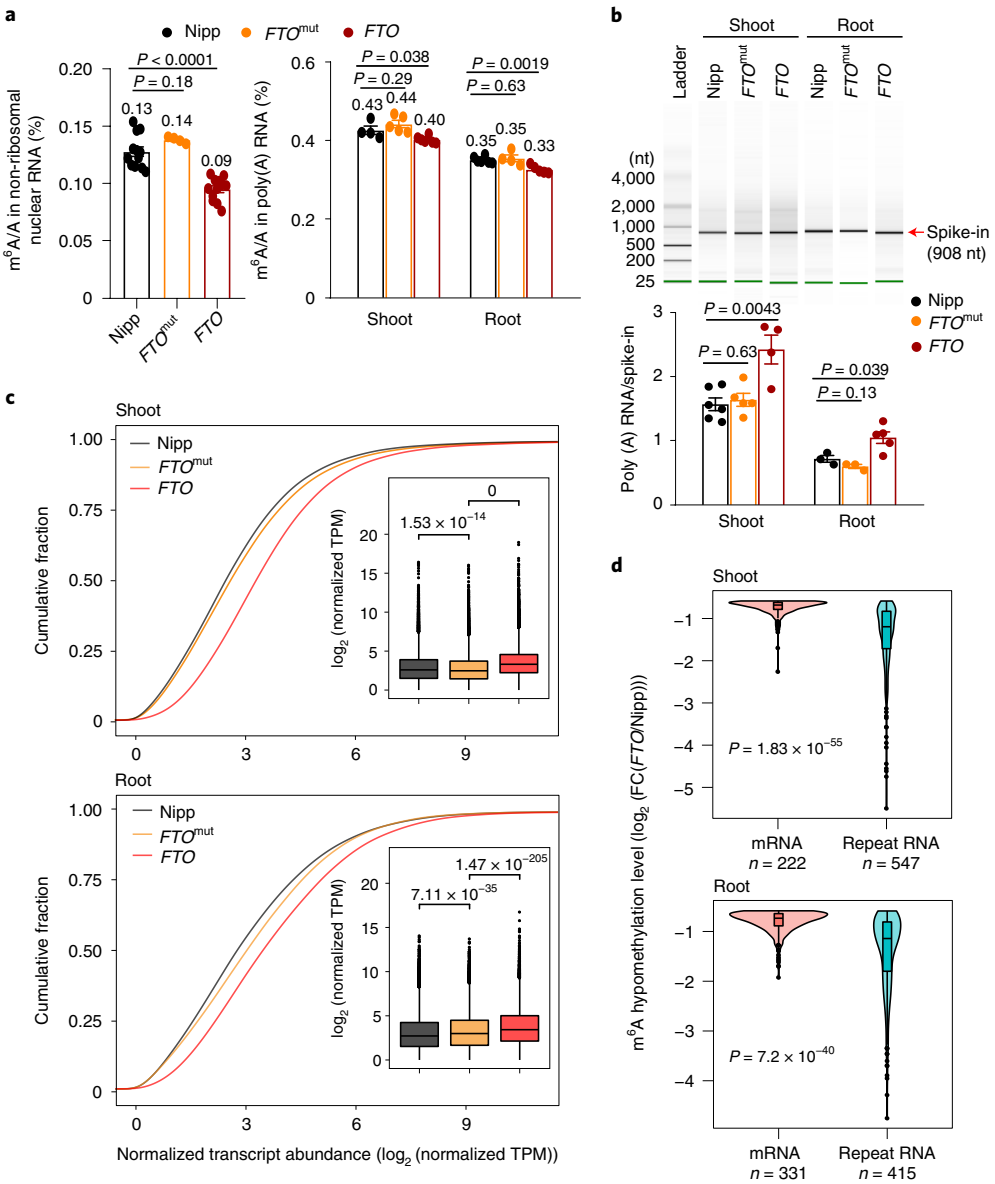


**Fig. 3 | Transcriptome-wide identification and analysis of FTO-mediated m$^6$A-demethylation sites in rice. a**, Quantification of the m$^6$A/A ratio in non-ribosomal nuclear RNA (left) and poly(A) RNA (right) isolated from 15-d-old WT (Nipp), *FTO*$^{mut}$- and *FTO*-transgenic rice shoots, roots and whole seedlings by LC–MS/MS. Data are mean ± s.e.m. ($n = 12$ Nipp, $n = 4$ *FTO*$^{mut}$, $n = 12$ *FTO* (left); $n = 4$ Nipp, $n = 5$ *FTO*$^{mut}$, $n = 6$ *FTO* in shoots; $n = 6$ Nipp, $n = 4$ *FTO*$^{mut}$, $n = 5$ *FTO* in roots (right)). **b**, Quantification of the ratio of poly(A) RNA to a synthesized poly(A) RNA spike-in control in a total RNA Pico Chip analysis using an Agilent 2100 Bioanalyzer. Poly(A) RNA along with the spike-in control were isolated from the same mass of shoots and roots of 15-d-old WT (Nipp), *FTO*$^{mut}$- and *FTO*-transgenic rice. Data are mean ± s.e.m. ($n = 6$ Nipp, $n = 5$ *FTO*$^{mut}$, $n = 4$ *FTO* in shoots; $n = 3$ Nipp and *FTO*$^{mut}$, $n = 5$ *FTO* in roots). *P* values are from unpaired, two-tailed *t*-tests. nt, nucleotides. **c**, Cumulative frequency plots and box plots showing the distribution of transcript expression in WT (Nipp), *FTO*$^{mut}$- and *FTO*-transgenic rice shoot (top) or root (bottom) tissues. In box plots, lower and upper hinges represent first and third quartiles, the center line represents the median, and whiskers represent ±1.5× the interquartile range. *P* values were determined using one-tailed Mann–Whitney *U*-tests. TPM, transcripts per million. **d**, Violin-and-box plots displaying the distribution of significant m$^6$A hypomethylation levels ($\log_2$(FC) < −0.5850) in mRNA and repeat RNA in shoots and roots of *FTO*-transgenic rice plants. In box plots, lower and upper hinges represent first and third quartiles, the center line represents the median, and whiskers represent ±1.5× the interquartile range. *P* values were determined using two-tailed Mann–Whitney *U*-tests.

for all poly(A) RNA and non-ribosomal RNA (Supplementary Fig. 14a–d). Consistently, m$^6$A levels in poly(A) RNA were also notably reduced in *FTO*-transgenic potato plants (Supplementary Fig. 14e). We further determined m$^6$A levels in U6 snRNA isolated from shoots and roots of WT, *FTO*$^{mut}$ and *FTO* rice and found that FTO expression did not mediate demethylation of m$^6$A in rice U6 snRNA (Supplementary Fig. 14f).

Considering that FTO can demethylate other RNA modifications (m$^6$A$_m$ and m$^1$A in different RNA types) in mammalian cells[16–18] and *N*$^6$-methyldeoxyadenosine (6mA) in single-stranded DNA in vitro[15], we subsequently investigated whether RNA modifications m$^6$A$_m$ and m$^1$A and DNA 6mA could be demethylated by FTO in *FTO*-expressing plants. We found that plants contained neither the homolog of human cap m$^6$A$_m$ methyltransferase PCIF1

(ref. [37]) (Supplementary Fig. 15a) nor cap $m^6A_m$ in rice poly(A) RNA (Supplementary Fig. 15b). Cap and internal $m^6A_m$ in U1 and U2 snRNA, $m^1A$ in tRNA and DNA 6mA are not substrates of expressed FTO in *FTO*-transgenic plants (Supplementary Fig. 16a–h and Methods). More discussion on the demethylation substrates of FTO is provided in the Supplementary Results. Collectively, these results indicate that FTO notably demethylates $m^6A$ in poly(A) RNA, non-ribosomal RNA and non-ribosomal nuclear RNA in *FTO*-transgenic plants.

**FTO mediates $m^6A$ demethylation of mRNA and repeat RNA.** We subsequently investigated potential molecular mechanisms through which FTO-mediated $m^6A$ demethylation may confer the observed profound increases in multiple economically impactful agronomic traits. We performed $m^6A$ methylated RNA immunoprecipitation (MeRIP) sequencing, calibrated using synthesized $m^6A$-modified poly(A) RNA spike-in controls in equal masses of shoot and root materials from 15-d-old WT, *FTO*$^{mut}$ and *FTO* rice plants. Calibrated $m^6A$ sequencing analysis in shoots and roots of WT, *FTO*$^{mut}$- and *FTO*-transgenic rice identified ~12,000 $m^6A$ peaks in each genotype, with good reproducibility across replicates (Supplementary Fig. 17a and Methods). The $m^6A$ motif and the distribution of detected $m^6A$ sites along transcripts were consistent with previous $m^6A$ sequencing results in plants[24,26,29] (Supplementary Fig. 17b). We then analyzed differentially methylated $m^6A$ sites in mRNA. Compared to those of WT rice, both shoots and roots of *FTO*-transgenic rice showed more hypomethylated $m^6A$ peaks (hypo-$m^6A$, 222 in shoots and 331 in roots) than hypermethylated $m^6A$ peaks (hyper-$m^6A$, 63 in shoots and 127 in roots) in mRNA (Supplementary Fig. 17c and Supplementary Data 1). The increased hypo-$m^6A$ peak number in mRNA in both shoots and roots of *FTO*-transgenic rice is consistent with the $m^6A$-demethylation function of FTO. Hypo-$m^6A$ peaks in mRNA were highly enriched within coding sequences and 3′ untranslated regions (Supplementary Fig. 18a and Supplementary Data 1). Gene ontology (GO) analysis of these hypo-$m^6A$-modified transcripts in shoots (222 genes) and roots (330 genes) of *FTO*-transgenic rice revealed enrichments for functional annotations related to 'cellular homeostatic process', 'one-carbon and small-molecule metabolic process' and 'gene expression' (Supplementary Fig. 18b and Supplementary Data 1). By contrast, no pathway enrichment was detected in our GO analyses of hypo-$m^6A$-containing genes from *FTO*$^{mut}$-transgenic shoots (31 genes) or roots (337 genes) (Supplementary Fig. 17c and Supplementary Data 1 and 2), suggesting that variant $m^6A$ peaks in *FTO*$^{mut}$ plants are apparently random and non-functional.

The RNA modification $m^6A$ was shown to be deposited onto chromatin-associated regulatory RNA (carRNA), including promoter-associated RNA, enhancer RNA and RNA transcribed from transposable elements (repeat RNA); further, $m^6A$ was shown to promote the degradation of a subset of these repeat RNA species through nuclear exosome-targeting-mediated nuclear degradation[38]. Mammalian repeat RNA species, such as those in the long interspersed element 1 (LINE1) family, are known to affect chromatin remodeling and gene transcription[39,40]; removal of $m^6A$ from LINE1 protects it from nuclear degradation and subsequently enhances both chromatin openness and downstream transcription in mouse embryonic stem cells[38]. Considering that repeat RNA such as mammalian LINE1 contains a poly(A) tail, we asked whether FTO expressed in rice could demethylate $m^6A$ in repeat RNA.

Compared to WT, 547 and 415 hypo-$m^6A$ peaks, representing 408 and 323 repeat RNA species, were respectively identified in shoots and roots of *FTO* rice (Supplementary Fig. 19a and Supplementary Data 1). We found that the extent of $m^6A$ hypomethylation was more pronounced for repeat RNA than that for mRNA (Fig. 3d and Supplementary Data 1). We ranked repeat classes or families according to their $m^6A$ hypomethylation levels, which showed that MuDR and En-Spm are the most strongly affected repeat RNA classes or families in *FTO* shoots and roots, respectively (Supplementary Fig. 19b and Supplementary Data 1).

**FTO induces transcriptional activation and more open chromatin.** Over the course of poly(A) RNA-purification steps during sample preparation for $m^6A$ detection by LC–MS/MS, we repeatedly noted that, even though we started with equal masses of *FTO*-transgenic and WT samples, *FTO*-transgenic plants consistently yielded higher amounts of poly(A) RNA (Supplementary Fig. 20a). To verify this, we isolated poly(A) RNA from samples of equal plant mass along with a synthesized poly(A) RNA spike-in control and quantified the ratio of poly(A) RNA to spike-in RNA by total RNA Pico Chip analysis using an Agilent 2100 Bioanalyzer. *FTO*-transgenic plants accumulated higher levels of poly(A) RNA than WT and *FTO*$^{mut}$ plants (Fig. 3b, Supplementary Fig. 20b–e and Methods). We next asked whether FTO affects plant ploidy, which could potentially explain the enhanced accumulation of transcripts; polyploidy has been a major force in plant evolution and crop domestication and has been harnessed for crop improvement[41]. Measurement of DNA content per cell nucleus by flow cytometry showed that *FTO*-transgenic rice was diploid, the same as WT and *FTO*$^{mut}$ plants (Supplementary Fig. 21).

Seeking biological insights about the regulation network(s) through which the FTO-mediated $m^6A$ demethylation enhances the accumulation of transcripts and affects yield and biomass phenotypes, we sampled equal masses of shoot and root materials from 15-d-old WT, *FTO*$^{mut}$ and *FTO* rice plants and performed quantitative RNA sequencing (RNA-seq) with an External RNA Controls Consortium (ERCC) RNA spike-in control. Quantitative RNA-seq analysis confirmed that *FTO*-transgenic plants did indeed accumulate higher overall levels of poly(A) RNA compared to WT and *FTO*$^{mut}$ plants (Fig. 3c, Supplementary Fig. 22, Supplementary Data 3 and Methods), further supporting our earlier observations (from RNA extractions) of increased poly(A) RNA expression in *FTO* plants.

Although $m^6A$ is known to increase transcript degradation[22,26,42], the relatively modest levels of hypo-$m^6A$-modified mRNA in *FTO*-transgenic rice shoots (222 genes) and roots (330 genes) may only contribute to a limited extent to overall increased mRNA levels in *FTO*-transgenic rice shoots and roots. We instead observed 11,342 and 6,933 significantly upregulated mRNA species (fold change (FC) > 1.5) in shoots and roots of *FTO* plants compared to those in WT control rice, respectively, from our quantitative RNA-seq experiment (Supplementary Fig. 23a and Supplementary Data 3). Increased overall expression levels of poly(A) RNA observed in *FTO*-transgenic rice shoots and roots are most likely derived from FTO-induced transcriptional activation.

Analysis of our quantitative RNA-seq data, focusing on differential expression of mRNA and repeat RNA, revealed that, compared to those of WT rice, shoots of *FTO* rice had 11,342 significantly upregulated mRNA species and 7,432 upregulated repeat RNA species (FC > 1.5) but had 539 significantly downregulated mRNA species and 918 downregulated repeat RNA species (FC < 2/3) (Supplementary Fig. 23a and Supplementary Data 3). Similar trends were also observed in *FTO* root samples: 6,933 significantly upregulated mRNA species and 7,068 upregulated repeat RNA species versus 2,699 significantly downregulated mRNA species and 2,009 downregulated repeat RNA species (Supplementary Fig. 23a and Supplementary Data 3). Overlap of these FTO-regulated mRNA or repeat RNA species between shoots and roots uncovered around 50% of overlapped transcripts, and their FTO-induced differential expression levels were organ specific (Supplementary Fig. 23b,c and Supplementary Data 3). These findings collectively suggest that, similar to the known biological impacts of mammalian

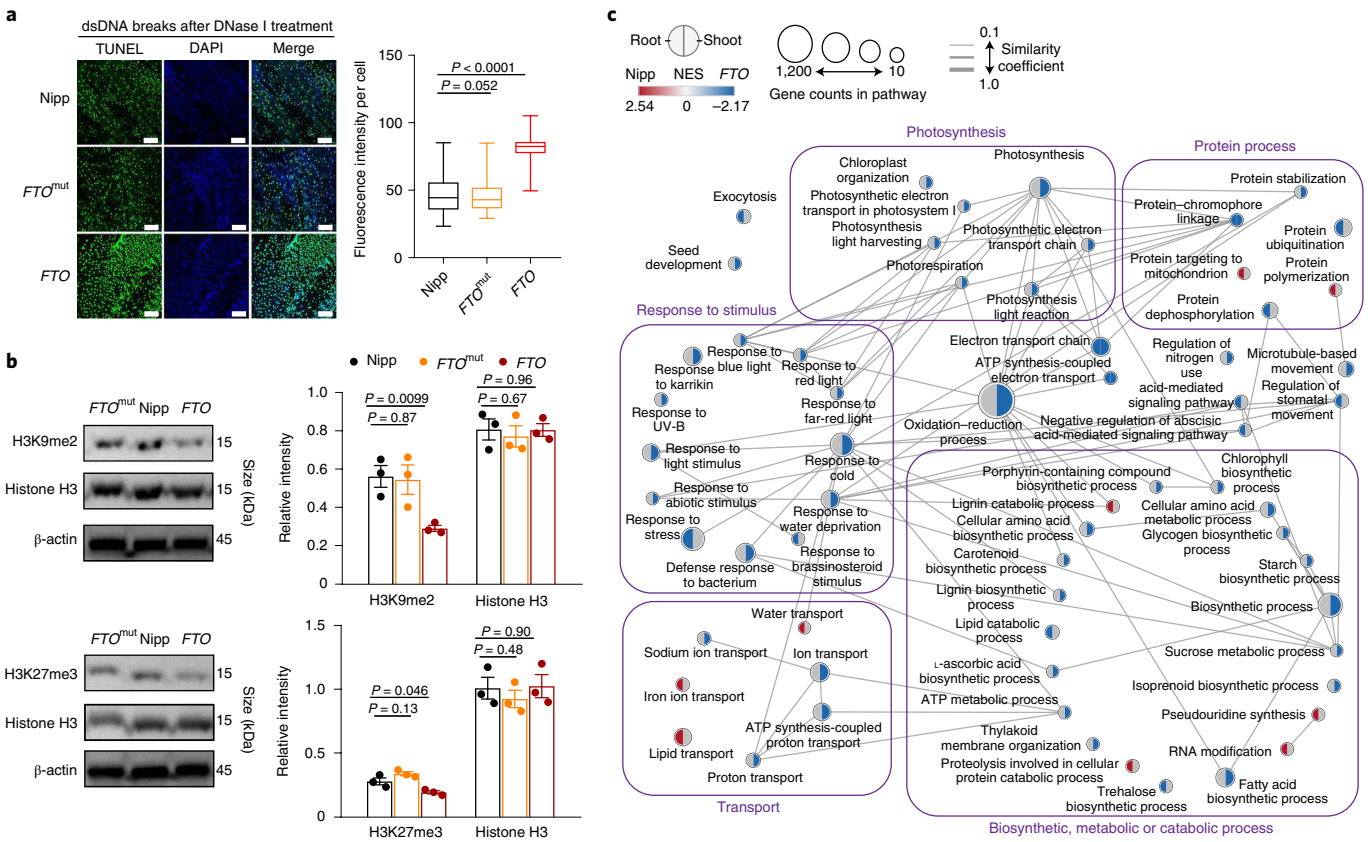


**Fig. 4 | FTO increases plant chromatin accessibility and affects various metabolic pathways. a**, DNase I-treated TUNEL assays in shoot apexes showing chromatin accessibility in 15-d-old *FTO*-transgenic rice compared with WT (Nipp) and *FTO*$^{mut}$-transgenic rice plants. Nuclei were stained with 4,6-diamidino-2-phenylindole (DAPI). Scar bars, 20 μm. Data are mean ± s.e.m., $n = 10$ biological replicates. *P* values are from unpaired, two-tailed *t*-tests. **b**, Immunoblot assays of H3K9me2 and H3K27me3 levels in 15-d-old *FTO*-transgenic rice compared with those in WT (Nipp) and *FTO*$^{mut}$-transgenic rice plants. The histone H3 level was quantified relative to the β-actin level; H3K9me2 and H3K27me3 levels were quantified relative to the histone H3 level. Data are mean ± s.e.m., $n = 3$. *P* values are from unpaired, two-tailed *t*-tests. **c**, GSEA network analysis of upregulated (normalized enrichment score (NES) < 0) and downregulated (NES > 0) pathways in shoots and roots of *FTO*-transgenic rice. Each pie chart represents a pathway; colors in pies indicate NES of pathways; positive and negative NESs indicate gene set enrichment in pathways of Nipp and *FTO*-transgenic rice, respectively; insignificantly enriched pathways (false discovery rate (FDR) > 0.1) are colored in gray; and left and right halves of each pie, respectively, represent pathways enriched in roots or shoots. Pie size indicates the number of genes in the pathway. Edges represent overlap between pathways, and the width represents the number of genes that overlap. To simplify the network, only edges meeting the cutoff (similarity coefficient >0.1) are shown.

m$^6$A in modifying transcriptional activation[38], FTO-mediated m$^6$A demethylation of plant repeat RNA may change the chromatin state. This can help to explain the global transcriptional upregulation that we observed in *FTO*-transgenic plants.

To validate whether the demethylation activity of FTO can affect chromatin state in plants, we performed DNase I-treated terminal deoxynucleotidyl transferase dUTP nick end labeling (TUNEL) assays on shoot apexes and found a notable increase in chromatin openness in *FTO*-transgenic rice compared to that in WT and *FTO*$^{mut}$ plants (Fig. 4a and Methods). Moreover, both *FTO*-transgenic rice and potato plants showed markedly decreased levels of histone 3 lysine 9 dimethyl (H3K9me2) and histone 3 lysine 27 trimethyl (H3K27me3) (both known transcription-repressing marks), suggesting that a more open chromatin state was indeed induced in *FTO* plants (Fig. 4b and Supplementary Fig. 24). These results confirm that FTO-mediated m$^6$A-demethylation promotes a more open chromatin state and induces transcriptional activation. This process could be through m$^6$A-modified repeat RNA or other carRNA species that affect chromatin state as recently shown in mammals[38,43–45].

We also investigated potential involvement of transcriptional activation programs in the observed high-yield and biomass phenotypes of *FTO*-transgenic rice. Gene set enrichment analysis (GSEA) between WT and *FTO*-transgenic rice shoots and roots revealed that many plant functional pathways were upregulated in *FTO*-transgenic rice, including pathways related to photosynthesis, ATP synthesis-coupled electron transport and regulation of nitrogen use (Fig. 4c and Supplementary Data 4). GSEA analysis also unveiled that most FTO-induced pathways were shoot- or root-specific (Fig. 4c). Thus, FTO-mediated m$^6$A-demethylation upregulates organ-specific transcripts associated with these pathways and transduces their downstream regulatory effects in our observed specific plant development and physiology, which coordinately increase crop yield and biomass.

## Discussion

In summary, we achieved dramatic induction of both crop yield and plant biomass for both monocot and eudicot plants under agricultural field conditions by expressing the human FTO protein in plants. Mechanistically, we detected no cap m$^6$A$_m$ in rice poly(A) RNA, consistent with our previous report on *Arabidopsis*[26]. Instead, we found that FTO mediates m$^6$A demethylation of both mRNA and repeat RNA in plants. The introduction of FTO caused elevated overall poly(A) RNA production and more open chromatin in plant

cells. Elevated tissue-specific mRNA species encoding proteins play functional roles in root cell proliferation, tiller formation and photosynthetic efficiency, contributing to elevating crop yield and biomass.

We observed notably elevated repeat RNA species upon transgenic expression of FTO in plants. We propose that FTO-mediated demethylation of some of these repeat RNA species and other car-RNA species could drive chromatin opening, as chromatin regulation by repeat RNA methylation has recently been reported in mammals[38,43–45]. Thus, beyond its empirical demonstration that expressing an RNA demethylase in plants dramatically boosts arguably the most important agronomic trait (yield) to increase agricultural productivity, our study represents a starting point for scientific investigations about the mechanisms by which RNA m$^6$A dynamics may regulate chromatin and gene transcription in plants.

## Online content

Any methods, additional references, Nature Research reporting summaries, source data, extended data, supplementary information, acknowledgements, peer review information; details of author contributions and competing interests; and statements of data and code availability are available at https://doi.org/10.1038/s41587-021-00982-9.

Received: 10 September 2019; Accepted: 11 June 2021;
Published online: 22 July 2021

## References

1. Godfray, H. C. J. et al. Food security: the challenge of feeding 9 billion people. *Science* **327**, 812–818 (2010).
2. Bailey-Serres, J., Parker, J. E., Ainsworth, E. A., Oldroyd, G. E. D. & Schroeder, J. I. Genetic strategies for improving crop yields. *Nature* **575**, 109–118 (2019).
3. Vaeck, M. et al. Transgenic plants protected from insect attack. *Nature* **328**, 33–37 (1987).
4. Rao, V. S. *Transgenic Herbicide Resistance in Plants* (CRC Press, 2014).
5. Wang, J. et al. A single transcription factor promotes both yield and immunity in rice. *Science* **361**, 1026–1028 (2018).
6. Wang, Y. & Li, J. Molecular basis of plant architecture. *Annu. Rev. Plant Biol.* **59**, 253–279 (2008).
7. Miura, K. et al. *OsSPL14* promotes panicle branching and higher grain productivity in rice. *Nat. Genet.* **42**, 545–549 (2010).
8. Li, S. et al. Modulating plant growth—metabolism coordination for sustainable agriculture. *Nature* **560**, 595–600 (2018).
9. South, P. F., Cavanagh, A. P., Liu, H. W. & Ort, D. R. Synthetic glycolate metabolism pathways stimulate crop growth and productivity in the field. *Science* **363**, eaat9077 (2019).
10. Frye, M., Harada, B. T., Behm, M. & He, C. RNA modifications modulate gene expression during development. *Science* **361**, 1346–1349 (2018).
11. Dominissini, D. et al. Topology of the human and mouse m$^6$A RNA methylomes revealed by m$^6$A-seq. *Nature* **485**, 201–206 (2012).
12. Meyer, K. D. et al. Comprehensive analysis of mRNA methylation reveals enrichment in 3′UTRs and near stop codons. *Cell* **149**, 1635–1646 (2012).
13. Geula, S. et al. m$^6$A mRNA methylation facilitates resolution of naive pluripotency toward differentiation. *Science* **347**, 1002–1006 (2015).
14. Frayling, T. M. et al. A common variant in the *FTO* gene is associated with body mass index and predisposes to childhood and adult obesity. *Science* **316**, 889–894 (2007).
15. Jia, G. et al. $N^6$-methyladenosine in nuclear RNA is a major substrate of the obesity-associated FTO. *Nat. Chem. Biol.* **7**, 885–887 (2011).
16. Mauer, J. et al. Reversible methylation of m$^6$A$_m$ in the 5′ cap controls mRNA stability. *Nature* **541**, 371–375 (2017).
17. Wei, J. et al. Differential m$^6$A, m$^6$A$_m$, and m$^1$A demethylation mediated by FTO in the cell nucleus and cytoplasm. *Mol. Cell* **71**, 973–985 (2018).
18. Mauer, J. et al. FTO controls reversible m$^6$A$_m$ RNA methylation during snRNA biogenesis. *Nat. Chem. Biol.* **15**, 340–347 (2019).
19. Li, Z. et al. FTO plays an oncogenic role in acute myeloid leukemia as a $N^6$-methyladenosine RNA demethylase. *Cancer Cell* **31**, 127–141 (2017).
20. Zhong, S. et al. MTA is *an Arabidopsis* messenger RNA adenosine methylase and interacts with a homolog of a sex-specific splicing factor. *Plant Cell* **20**, 1278–1288 (2008).
21. Bodi, Z. et al. Adenosine methylation in *Arabidopsis* mRNA is associated with the 3′ end and reduced levels cause developmental defects. *Front. Plant Sci.* **3**, 48 (2012).
22. Shen, L. et al. $N^6$-methyladenosine RNA modification regulates shoot stem cell fate in *Arabidopsis*. *Dev. Cell* **38**, 186–200 (2016).
23. Růžička, K. et al. Identification of factors required for m$^6$A mRNA methylation in *Arabidopsis* reveals a role for the conserved E3 ubiquitin ligase HAKAI. *New Phytol.* **215**, 157–172 (2017).
24. Zhang, F. et al. The subunit of RNA $N^6$-methyladenosine methyltransferase OsFIP regulates early degeneration of microspores in rice. *PLoS Genet.* **15**, e1008120 (2019).
25. Zheng, G. et al. ALKBH5 is a mammalian RNA demethylase that impacts RNA metabolism and mouse fertility. *Mol. Cell* **49**, 18–29 (2013).
26. Duan, H. C. et al. ALKBH10B is an RNA $N^6$-methyladenosine demethylase affecting *Arabidopsis* floral transition. *Plant Cell* **29**, 2995–3011 (2017).
27. Martinez-Perez, M. et al. *Arabidopsis* m$^6$A demethylase activity modulates viral infection of a plant virus and the m$^6$A abundance in its genomic RNAs. *Proc. Natl Acad. Sci. USA* **114**, 10755–10760 (2017).
28. Scutenaire, J. et al. The YTH domain protein ECT2 is an m$^6$A reader required for normal trichome branching in *Arabidopsis*. *Plant Cell* **30**, 986–1005 (2018).
29. Wei, L. H. et al. The m$^6$A reader ECT2 controls trichome morphology by affecting mRNA stability in *Arabidopsis*. *Plant Cell* **30**, 968–985 (2018).
30. Arribas-Hernández, L. et al. An m$^6$A-YTH module controls developmental timing and morphogenesis in *Arabidopsis*. *Plant Cell* **30**, 952–967 (2018).
31. Arribas-Hernández, L. et al. Recurrent requirement for the m$^6$A-ECT2/ECT3/ECT4 axis in the control of cell proliferation during plant organogenesis. *Development* **147**, dev189134 (2020).
32. Hou, Y. et al. CPSF30-L-mediated recognition of mRNA m$^6$A modification controls alternative polyadenylation of nitrate signaling-related gene transcripts in *Arabidopsis*. *Mol. Plant* **14**, 688–699 (2021).
33. Song, P. et al. *Arabidopsis* $N^6$-methyladenosine reader CPSF30-L recognizes FUE signal to control polyadenylation site choice in liquid-like nuclear body. *Mol. Plant* **14**, 571–587 (2021).
34. Wu, J., Peled-Zehavi, H. & Galili, G. The m$^6$A reader ECT2 post-transcriptionally regulates proteasome activity in *Arabidopsis*. *New Phytol.* **228**, 151–162 (2020).
35. Li, X. et al. Control of tillering in rice. *Nature* **422**, 618–621 (2003).
36. Pirasteh-Anosheh, H., Saed-Moucheshi, A., Pakniyat, H. & Pessarakli, M. Stomatal responses to drought stress. in *Water Stress and Crop Plants: A Sustainable Approach* 24–40 (Wiley, 2016).
37. Akichika, S. et al. Cap-specific terminal $N^6$-methylation of RNA by an RNA polymerase II-associated methyltransferase. *Science* **363**, eaav0080 (2019).
38. Liu, J. et al. $N^6$-methyladenosine of chromosome-associated regulatory RNA regulates chromatin state and transcription. *Science* **367**, 580–586 (2020).
39. Jachowicz, J. W. et al. LINE-1 activation after fertilization regulates global chromatin accessibility in the early mouse embryo. *Nat. Genet.* **49**, 1502–1510 (2017).
40. Percharde, M. et al. A LINE1–nucleolin partnership regulates early development and ESC identity. *Cell* **174**, 391–405 (2018).
41. Sattler, M. C., Carvalho, C. R. & Clarindo, W. R. The polyploidy and its key role in plant breeding. *Planta* **243**, 281–296 (2016).
42. Wang, X. et al. $N^6$-methyladenosine-dependent regulation of messenger RNA stability. *Nature* **505**, 117–120 (2014).
43. Chelmicki, T. et al. m$^6$A RNA methylation regulates the fate of endogenous retroviruses. *Nature* **591**, 312–316 (2021).
44. Xu, W. et al. METTL3 regulates heterochromatin in mouse embryonic stem cells. *Nature* **591**, 317–321 (2021).
45. Liu, J. et al. The RNA m$^6$A reader YTHDC1 silences retrotransposons and guards ES cell identity. *Nature* **591**, 322–326 (2021).

## Methods

**Plasmid construction and plant transformation.** Native human *FTO* cDNA (GenBank accession no. NP_001073901.1) and optimized *FTO* cDNA with codon optimization in rice were subcloned into the binary vector pCAMBIA1307 carrying the CaMV *35S* promoter between HindIII and KpnI restriction sites with sequence for C-terminal 1×Flag, generating the plasmids *35S::FTO-Flag* and *35S::optFTO-Flag*, respectively. Double mutation of *FTO* (resulting in R316Q and R322Q) was performed using the Agilent QuikChange II XL Site-Directed Mutagenesis kit (Agilent, 200521) to obtain the plasmid *35S::FTO$^{mut}$-Flag*. For rice transformation, two plasmids, *35S::FTO-Flag* and *35S::FTO$^{mut}$-Flag*, and one plasmid, *35S::optFTO-Flag*, were respectively transformed into Nipp and ZH11 plants using *Agrobacterium tumefaciens* strain EHA105 according to a published method[46]. Medium supplemented with hygromycin was used to select transformants. Twenty independent $T_0$ transformations were generated to produce $T_1$ progeny. T-DNA copy number (CN) was determined in $T_1$ plants by quantitative PCR with reverse transcription analysis using forward and reverse primers for *HPT* (hygromycin phosphotransferase) and *SPS* (sucrose phosphate synthase) according to published methods[47,48]. At least three independent transformation lines with one CN of the target gene were selected and produced $T_2$ progeny (Supplementary Tables 1 and 2). Non-single insert lines were not further characterized. Homozygous lines were confirmed in $T_2$ offspring by genomic PCR, testing for the presence of both *HPT* and *FTO* using the primers *HPT*-gDNA PCR forward and reverse and *FTO*-gDNA PCR forward and reverse, respectively.

For potato transformation, the plasmid *35S::FTO-Flag* was transformed into EM3 using *A. tumefaciens* GV3101 according to a published method[49]. Medium supplemented with hygromycin was used to select transformants. Transgenic plants were tested by genomic PCR in the $T_1$ generation for the presence of both *HPT* and *FTO* using the same primers described above. T-DNA CN was determined in $T_1$ plants by quantitative PCR with reverse transcription analysis using the primers *HPT*-CN forward and reverse and *Urease*-CN forward and reverse according to published methods[47,50]. Transgenic lines with one CN insertion were used for further study (Supplementary Tables 3 and 4). All primers used for plasmid construction and transgenic line verification are listed in Supplementary Table 5.

**Field experiments.** Single-copy insert and homozygous *FTO*-transgenic rice plants (*FTO-1*, *FTO-2*, *FTO-4*, *FTO-5* and *FTO*$^{mut}$ in the Nipp background; *FTO-3* in the ZH11 background) along with WT Nipp and ZH11 plants were grown in standard paddy conditions during normal rice planting seasons in Beijing (N 40° 06′ 13.07″, E 116° 25′ 6.34″) and Jiangxi (N 28° 22′, E 115° 55′), China. The planting density was 15 cm in a row and 17 cm between rows with one plant per hill. Normal field management including irrigation, fertilization and disease control was carried out following normal agricultural practices in rice cultivation. Harvested grains were air dried and stored at room temperature. Yield per plant, total grain number per plant, biomass per plant, effective tiller number per plant, plant height, spike length, total grain number per major panicle and 1,000-grain weight were determined after harvesting. Values are mean ± s.e.m.

WT (EM3) and *FTO*-transgenic potato plants were grown in the field in the normal potato-planting season in Hebei (N 39° 27′, E 115° 51′), China. The planting density was 30 × 30 cm with one bud per hill in a ridging planting mode. The ridge height was about 30 cm, and the ridge width was about 60 cm. Normal field management including irrigation, fertilization and disease control was carried out following normal agricultural practices in potato cultivation. Tuber weight and tuber number per plot were determined after harvesting.

**Measurement of photosynthesis parameters.** Photosynthesis parameters were measured using a LI-6800 system (LI-COR) in flag leaves of Nipp, *FTO*$^{mut}$- and *FTO*-transgenic rice at the heading stage grown in the field from 9:00 to 11:30 and from 14:00 to 16:30 under a daily photoperiod of 12 h of light and 12 h of dark with 55–60% humidity[51].

**Root morphological analysis.** Plants were harvested at the tillering stage (3 months after planting in soil) and the seedling stage (15 d after growth under hydroponic conditions). All visible roots of one plant were carefully collected. After washing to be free of soil, cleaned roots were dispersed in water in a transparent tray (30 × 20 × 3 cm) and scanned using an Epson scanner (Epson Expression, 1600 Pro) to acquire root images. Root images were then analyzed with WinRHIZO software (Regent Instruments) to determine root morphological parameters such as root length and root number[52].

**Histological analysis.** Rice lateral root tips were stained with PI for 1 min and then imaged using a Zeiss LSM 700 laser scanning confocal microscope. Root apical meristem size and meristem cell length and number were determined according to the file of cortex cells from confocal microscopy images[53]. Shoot apical meristem size and L1 cell number were calculated according to a previous report[54]. Paraffin sections of rice as well as potato tissues were immersed in xylene to remove paraffin and rehydrated with a series of ethanol solutions. After washing with water, sections were stained with Safranin O (Coolaber) and Fast Green (Coolaber)[55] and imaged under bright field through a microscope (Olympus, IX73). Tiller buds at shoot basal regions of four-leaf-stage seedlings were imaged under bright field through a microscope (Nikon, SMZ18).

**EdU staining.** EdU staining was performed as previously reported[56] with modifications. Four-day-old seedlings were immersed in a 100 μM EdU solution for 6 h. After fixation for 30 min in 4% formaldehyde, the EdU-detection cocktail was made according to the protocol from the Click-iT EdU Alexa Fluor 488 Imaging kit (C10083, Invitrogen). Images were captured using a Zeiss LSM 700 laser scanning confocal microscope, and numbers of EdU-stained cells in rice root meristems were quantified using ImageJ software.

**Isolation of poly(A) RNA, non-ribosomal RNA, non-ribosomal nuclear RNA, tRNA and U1, U2 and U6 snRNA.** Total RNA was isolated with the TRIzol reagent (Invitrogen). Poly(A) RNA was isolated with Dynabeads oligo$(dT)_{25}$ (Thermo Fisher Scientific) following the manufacturer's protocol. Non-ribosomal RNA was extracted from total RNA via removal of rRNA using the Ribo-Zero rRNA Removal kit (Illumina) following the manufacturer's protocol. Non-ribosomal nuclear RNA was isolated from total nuclear RNA via removal of rRNA using the Ribo-Zero rRNA Removal kit (Illumina) after total nuclear RNA extraction from plant nuclei with the TRIzol reagent (Invitrogen). For isolation of total tRNA, the small RNA fraction (<200 nucleotides) was isolated from total RNA using the RNA Clean & Concentrator-5 kit (Zymo Research, R1016) and separated on a 15% TBE–urea gel, and total tRNA bands were sliced and recovered from the gel[17]. For isolation of U1, U2 and U6 snRNA, the small RNA fraction (<200 nucleotides) was separated on a 6% TBE–urea gel, and bands corresponding to U1, U2 and U6 snRNA[17,18] were sliced and recovered from the gel. RNA concentration was measured with the Qubit 2.0 (Thermo Fisher Scientific) and the Equalbit RNA HS Assay kit (Vazyme, EQ211–02). The quality of all isolated types of RNA was confirmed using an Agilent 2100 Bioanalyzer instrument (Agilent).

**LC–MS/MS quantification of $m^6A$, $m^1A$, $m^6A_m$ and 6mA.** For quantification of $m^6A$, 100 ng RNA (including poly(A) RNA, non-ribosomal RNA, non-ribosomal nuclear RNA and U6 snRNA) was digested with 1 U Nuclease P1 (Wako, 145-08221) in 20 μl buffer containing 10 mM ammonium acetate (pH 5.3) at 42 °C for 4 h, followed by the addition of 1 U Shrimp Alkaline Phosphatase (NEB, M0371L) and 100 mM MES (pH 6.5) at 37 °C for 4 h. After centrifuging at 15,000 r.p.m. for 10 min, supernatants of digested samples were injected into an LC–MS/MS system for analysis. For quantification of $m^1A$ in tRNA[17], 200 ng tRNA was digested with 1 U Nuclease P1 (Wako, 145-08221) in 40 μl buffer containing 10 mM ammonium acetate (pH 5.3) at 60 °C for 2 h, followed by the addition of 1 U Shrimp Alkaline Phosphatase (NEB, M0371L) and 100 mM MES (pH 6.5) at 37 °C for 3 h. After centrifuging at 15,000 r.p.m. for 10 min, supernatants of digested samples were injected into an LC–MS/MS system for analysis. For quantification of total $m^6A_m$ (cap and internal) and internal $m^6A_m$ in poly(A) RNA and snRNA, according to previous reports[17,18], 100 ng poly(A) RNA and U1 and U2 snRNA was decapped with 10 U RppH (NEB, M0356S) in NEB ThermoPol buffer (NEB, B9004S) for 3 h at 37 °C. RNA after decapping (for quantification of total $m^6A_m$) and RNA without decapping (for quantification of internal $m^6A_m$) were subsequently digested with 1 U Nuclease P1 (Wako, 145-08221) in 20 μl buffer containing 10 mM ammonium acetate (pH 5.3) at 42 °C for 4 h, followed by the addition of 1 U Shrimp Alkaline Phosphatase (NEB, M0371L) and 100 mM MES (pH 6.5) at 37 °C for 4 h. After centrifuging at 15,000 r.p.m. for 10 min, supernatants of digested samples were injected into an LC–MS/MS system for analysis. For quantification of cap $m^6A_m$ in snRNA according to a previous report[18], 100 ng U1 and U2 snRNA was decapped with 25 U RppH (NEB, M0356S) in NEB ThermoPol buffer (NEB, B9004S) for 3 h at 37 °C. The 5′ phosphates of the exposed cap-adjacent base were removed by the addition of 5 U Shrimp Alkaline Phosphatase (NEB, M0371L) in 100 mM MES (pH 6.5) at 37 °C for 1 h. After phenol–chloroform extraction and ethanol precipitation, RNA samples were then digested with 1 U Nuclease P1 (Wako, 145-08221) in 20 μl buffer containing 10 mM ammonium acetate (pH 5.3) at 42 °C for 3 h. After centrifuging at 15,000 r.p.m. for 10 min, supernatants of digested samples were injected into an LC–MS/MS system for analysis.

For quantification of 6mA in genomic DNA[57], genomic DNA was purified from the chromatin of 15-d-old *FTO*-transgenic rice plants to avoid bacterial contamination. Chromatin was extracted according to a previously described protocol[58]. In total, 500 ng DNA was digested with 5 U DNA Degradase Plus (Zymo Research, E2021) in 40 μl 1× DNA Degradase Reaction Buffer at 37 °C overnight. After centrifuging at 15,000 r.p.m. for 10 min, supernatants of digested samples were injected into an LC–MS/MS system for analysis.

Nucleosides were separated by ultra-performance liquid chromatography (Shimadzu) on a Zorbax SB-Aq column (Shimadzu) with mass spectrometry detection using a Triple Quad 5500 mass spectrometer (AB SCIEX) in positive ion mode by multiple-reaction monitoring. MS parameters were optimized for $m^6A$, $m^1A$, $m^6A_m$ and 6mA detection. Nucleosides were quantified using nucleoside-to-base ion mass transitions of *m/z* 268.0 to 136.0 (A), *m/z* 282.0 to 150.1 ($m^6A$), *m/z* 282.0 to 150.1 ($m^1A$), *m/z* 296.0 to 150.0 ($m^6A_m$), *m/z* 266.1 to 150.1 (6mA) and *m/z* 252.1 to 136.1 (dA). $m^6A$/A, $m^6A_m$/A, $m^1A$/A and 6mA/dA ratios were calculated by fitting signal intensities to standard curves obtained from

a concentration series of pure nucleoside standards (Sigma-Aldrich) run with the same batch of samples.

**Quantitative analysis of poly(A) RNA isolation by Bioanalyzer.** A 908-nucleotide synthesized poly(A) RNA spike-in control was transcribed in vitro using the MEGAscript kit (AM1333, Thermo Fisher Scientific) (Supplementary Table 6). Total RNA was extracted from equal masses of 15-d-old rice shoots and roots using the TRIzol reagent (Invitrogen) and was added with the spike-in control (the same amount of spike-in for equal mass of tissue sample). Poly(A) RNA, along with the spike-in, was isolated using Dynabeads oligo$(dT)_{25}$ (Thermo Fisher Scientific) following the manufacturer's protocol and subsequently loaded in a total RNA Pico Chip (RNA 6000 Pico kit, 5067-1513, Agilent) using an Agilent 2100 Bioanalyzer Instrument (Agilent). The mimic gel and chromatograms of the isolated poly(A) RNA and the spike-in were obtained from the Agilent 2100 Bioanalyzer. The ratio of poly(A) RNA to spike-in was determined by calculating the peak area ratio of poly(A) RNA versus spike-in.

**Ploidy measurement using flow cytometry.** To examine the ploidy level of *FTO* plants in this analysis, fresh leaves were chopped with a sharp razor in precooled extraction buffer (0.1 M citric acid, 0.5% Tween-20, pH 2.3). After filtered through a 30-μm cell strainer, the DNA content per nucleus stained with DAPI was measured using the BD LSRFortessa cell analyzer according to a previous report[59].

**DNase I-treated TUNEL assay.** Paraffin sections of shoot apexes were immersed in xylene to remove paraffin and rehydrated with a series of ethanol solutions. After washing with water, sections were treated with 0.2 U $ml^{-1}$ DNase I digestion (NEB, M0303L) and then post-fixed with 4% formaldehyde. TUNEL assays were subsequently performed on fixed tissues using the DeadEnd Fluorometric TUNEL System (Promega) according to the manufacturer's instructions[38]. The nuclear area was stained with DAPI. Images were captured using a Zeiss LSM 700 laser scanning confocal microscope, and intensity of nuclear TUNEL signal was quantified using ImageJ software.

**Calibrated m$^6$A MeRIP sequencing.** Poly(A) RNA along with spike-in controls (5 pg) was isolated from equal masses (1 g) of 15-d-old shoots and roots of WT (Nipp), *FTO*$^{mut}$ and *FTO* plants from hydroponic experiments and subjected to m$^6$A MeRIP sequencing[11,12]. The mixture of spike-in controls contained three 20% m$^6$A-modified RNA species with different sequences and three non-m$^6$A-modified RNA species with different sequences (Supplementary Table 6), which were transcribed in vitro using a kit (AM1333, Thermo Fisher Scientific). Poly(A) RNA with spike-in controls was fragmented into molecules of ~100 nucleotides in length using RNA Fragmentation Reagents (Ambion) and subjected to m$^6$A immunoprecipitation using the EpiMark $N^6$-Methyladenosine Enrichment kit (NEB) following the manufacturer's protocol. Library preparation was performed using the NEBNext Ultra II Directional RNA Library Prep Kit for Illumina (NEB) according to the manufacturer's protocol. Sequencing was performed on an Illumina HiSeq 4000 machine in paired-end mode with 150 bp per read (Genewiz).

**Quantitative RNA sequencing.** Equal masses of 15-d-old shoots and roots of WT (Nipp), *FTO*$^{mut}$ and *FTO* plants from hydroponic experiments were used for quantitative RNA-seq. After total RNA isolation, ERCC RNA spike-in control (Ambion) was added to each isolated total RNA sample (0.1 μl per 5 mg of plant mass). Total RNA with spike-in controls was subjected to non-ribosomal RNA purification using the Ribo-Zero rRNA Removal kit (Illumina, MRZPL1224). After rRNA removal, purified non-ribosomal RNA was fragmented into molecules ~100 nucleotides in length using RNA Fragmentation Reagents (Ambion) according to the manufacturer's protocol. Library preparation was performed using the NEBNext Ultra II Directional RNA Library Prep Kit for Illumina (NEB) according to the manufacturer's protocols. Sequencing was performed on an Illumina HiSeq 4000 machine in paired-end mode with 150 bp per read (Genewiz).

**Calibrated m$^6$A-seq data analysis.** Adaptor sequences of raw reads were trimmed by Cutadapt version 1.15 (ref. [60]) Reads longer than 15 nucleotides after trimming were mapped to the rice genome (MSU 7.0) using HISAT2 version 2.1.0 (ref. [61]) with the following parameters: '-p 24–time–reorder–dta–no-unal–pen-noncansplice 12–rna-strandness RF -k 5'. mRNA and repeat RNA annotations were downloaded from the Rice Genome Annotation Project and the Rice Annotation Project Database, respectively. Mapped reads were separated by strands, and then MeTPeak[62] was used to detect m$^6$A peaks with mRNA and repeat RNA annotations ('FRAGMENT_LENGTH=200, READ_LENGTH=150, PEAK_CUTOFF_FDR=0.05, WINDOW_WIDTH=50, SLIDING_STEP=10, FOLD_ENRICHMENT=2'). Peaks overlapping between two replicates were merged and considered for further analysis. Counts of reads in union peaks from pairwise groups (Nipp versus *FTO*, Nipp versus *FTO*$^{mut}$) were calculated by featureCounts ('-t exon -g gene_id -C -M -O–fraction -T 24 -s 2 -p–readShiftType downstream–readShiftSize 100–read2pos 5') from Subread version 1.6.4 (ref. [63]). The number of reads mapped to all union peaks divided by the number of reads mapped to m$^6$A-modified spike-in controls represented the whole m$^6$A level. Next, fold enrichment of individual union peaks was normalized to $RPKM_{IP/input}$ based on the normalized whole m$^6$A level. Differential peaks were defined as those meeting the fold-change cutoff ($\log_2(FC) > 0.5850$ or $\log_2(FC) < -0.5850$) and read-density cutoff ($RPKM_{input} > 0.5$) in input samples. Motif enrichment from peaks was performed by HOMER version 4.9 (ref. [64]).

**Quantitative RNA-seq data analysis.** Adaptor sequences of raw reads were trimmed by Cutadapt version 1.15 (ref. [60]). Trimmed reads shorter than 16 nucleotides were discarded, and remaining reads were mapped to the rice genome (MSU 7.0) using HISAT2 version 2.1.0 (ref. [61]) with the above parameters. mRNA and repeat RNA annotations were downloaded from the Rice Genome Annotation Project and the Rice Annotation Project Database, respectively. Reads for mRNA and repeat RNA were counted by featureCounts ('-t exon -g gene_id -C -M -O–fraction -T 24 -s 2 -p') from Subread version 1.6.4 (ref. [63]) and then normalized to TPM values. TPM values were further normalized using RNA ERCC spike-in controls using the function 'normalize.loess' from the 'affy' package[65] according to a previous study[66]. Normalized TPM values were used for downstream analysis.

**Gene ontology and gene set enrichment analysis.** GO analysis on hypomethylated transcripts from *FTO*-transgenic rice shoot and root tissues compared to those of WT was performed using agriGO version 2.0 (ref. [67]). GSEA software[68] downloaded from the Broad Institute was employed for GSEA of RNA-seq data with the GO annotation set (http://ge-lab.org/gskb/7-plant-results-database/oryza_sativa_asian-rice_gmt2.gmt). Results (FDR < 0.1) were further organized into a network by EnrichmentMap[69].

**Statistical analysis.** Statistical analysis was conducted using GraphPad. Data are presented as mean ± s.e.m. Unpaired Student's *t*-tests were used for comparing agronomic traits of each transgenic line with those of the control.

**Reporting Summary.** Further information on research design is available in the Nature Research Reporting Summary linked to this article.

## Data availability

m$^6$A-seq and quantitative RNA-seq data generated by this study were deposited in the GEO database under the accession number GSE135549. Source data are provided with this paper.

## References


46. Toki, S. et al. Early infection of scutellum tissue with *Agrobacterium* allows high-speed transformation of rice. *Plant J.* **47**, 969–976 (2006).
47. Yang, L. et al. Estimating the copy number of transgenes in transformed rice by real-time quantitative PCR. *Plant Cell Rep.* **23**, 759–763 (2005).
48. Ding, J. et al. Validation of a rice specific gene, sucrose phosphate synthase, used as the endogenous reference gene for qualitative and real-time quantitative PCR detection of transgenes. *J. Agric. Food Chem.* **52**, 3372–3377 (2004).
49. Chetty, V. J., Narváez-Vásquez, J. & Orozco-Cárdenas, M. L. Potato (*Solanum tuberosum* L.). In *Agrobacterium Protocols* 3rd edn, Vol. 2 (ed Wang, K.), 85–96 (Springer, 2015).
50. Witte, C. P., Tiller, S., Isidore, E., Davies, H. V. & Taylor, M. A. Analysis of two alleles of the urease gene from potato: polymorphisms, expression, and extensive alternative splicing of the corresponding mRNA. *J. Exp. Bot.* **56**, 91–99 (2005).
51. Ambavaram, M. M. et al. Coordinated regulation of photosynthesis in rice increases yield and tolerance to environmental stress. *Nat. Commun.* **5**, 5302 (2014).
52. Wen, Z., Li, H., Shen, J. & Rengel, Z. Maize responds to low shoot P concentration by altering root morphology rather than increasing root exudation. *Plant Soil* **416**, 377–389 (2017).
53. Ioio, R. D. et al. A genetic framework for the control of cell division and differentiation in the root meristem. *Science* **322**, 1380–1384 (2008).
54. Yang, F. et al. A maize glutaredoxin gene, *abphyl2*, regulates shoot meristem size and phyllotaxy. *Plant Cell* **27**, 121–131 (2015).
55. Zhong, R., Taylor, J. J. & Ye, Z. H. Disruption of interfascicular fiber differentiation in *an Arabidopsis* mutant. *Plant Cell* **9**, 2159–2170 (1997).
56. Xu, L. et al. ABNORMAL INFLORESCENCE MERISTEM1 functions in salicylic acid biosynthesis to maintain proper reactive oxygen species levels for root meristem activity in rice. *Plant Cell* **29**, 560–574 (2017).
57. Zhou, C. et al. Identification and analysis of adenine $N^6$-methylation sites in the rice genome. *Nat. Plants* **4**, 554–563 (2018).
58. Saleh, A., Alvarez-Venegas, R. & Avramova, Z. An efficient chromatin immunoprecipitation (ChIP) protocol for studying histone modifications in *Arabidopsis* plants. *Nat. Protoc.* **3**, 1018–1025 (2008).
59. Yang, L., Wang, Z. & Hua, J. Measuring cell ploidy level in *Arabidopsis thaliana* by flow cytometry. *Methods Mol. Biol.* **1991**, 101–106 (2019).
60. Martin, M. Cutadapt removes adapter sequences from high-throughput sequencing reads. *EMBnet J.* **17**, 10–12 (2011).

61. Kim, D., Langmead, B. & Salzberg, S. L. HISAT: a fast spliced aligner with low memory requirements. *Nat. Methods* **12**, 357–360 (2015).
62. Cui, X., Meng, J., Zhang, S., Chen, Y. & Huang, Y. A novel algorithm for calling mRNA m$^6$A peaks by modeling biological variances in MeRIP-seq data. *Bioinformatics* **32**, i378–i385 (2016).
63. Liao, Y., Smyth, G. K. & Shi, W. The Subread aligner: fast, accurate and scalable read mapping by seed-and-vote. *Nucleic Acids Res.* **41**, e108 (2013).
64. Heinz, S. et al. Simple combinations of lineage-determining transcription factors prime *cis*-regulatory elements required for macrophage and B cell identities. *Mol. Cell* **38**, 576–589 (2010).
65. Gautier, L., Cope, L., Bolstad, B. M. & Irizarry, R. A. Affy—analysis of Affymetrix GeneChip data at the probe level. *Bioinformatics* **20**, 307–315 (2004).
66. Loven, J. et al. Revisiting global gene expression analysis. *Cell* **151**, 476–482 (2012).
67. Tian, T. et al. AgriGO v2.0: a GO analysis toolkit for the agricultural community, 2017 update. *Nucleic Acids Res.* **45**, W122–W129 (2017).
68. Subramanian, A. et al. Gene set enrichment analysis: a knowledge-based approach for interpreting genome-wide expression profiles. *Proc. Natl Acad. Sci. USA* **102**, 15545–15550 (2005).
69. Merico, D., Isserlin, R., Stueker, O., Emili, A. & Bader, G. D. Enrichment map: a network-based method for gene-set enrichment visualization and interpretation. *PLoS ONE* **5**, e13984 (2010).

## Acknowledgements

We thank Y. Wang for paraffin embedding station support, C. Xu for microtome support and X. Meng and J. Wang for assistance during field work. This work was supported by the National Basic Research Program of China (2019YFA0802201 and 2017YFA0505201 to G.J.), the National Natural Science Foundation of China (21822702, 21820102008, 92053109 and 21432002 to G.J.), the Beijing Natural Science Foundation (Z200010 to G.J.), EpiPlanta Biotech Ltd. (to G.J.), the Beijing Advanced Innovation Center for Genomics at Peking University (to G.J.) and the Zhong Ziyi Education Foundation (to C.H.). C.H. is a Howard Hughes Medical Institute Investigator.

## Author contributions

G.J. and C.H. conceived the original idea and designed original studies. Q.Y. performed most experiments with help from Y.L., Y. Xiao., S.Z., X.W., Y. Xu, Y.L., J.Y., J.T., H.-C.D., L.-H.W., Q.T., C.W., Wutong Zhang, Y.W., P.S., Q.L., Wei Zhang, S.D., H.Y., H.Z. and B.S. S.L. performed most computational analysis with help from J.W. G.J. and C.H. wrote the manuscript with input from Q.Y. and S.L.

## Competing interests

A patent application has been filed by EpiPlanta Biotech Ltd. for the technology disclosed in this publication. C.H. is a scientific founder and a member of the scientific advisory board of Accent Therapeutics.

## Additional information

**Supplementary information** The online version contains supplementary material available at https://doi.org/10.1038/s41587-021-00982-9.

**Correspondence and requests for materials** should be addressed to B.S., C.H. or G.J.

**Peer review information** *Nature Biotechnology* thanks Brian Gregory and the other, anonymous, reviewer(s) for their contribution to the peer review of this work.

**Reprints and permissions information** is available at www.nature.com/reprints.

nature research

Corresponding author(s): Baoan Song, Chuan He, Guifang Jia and NBT-RA48858C

Last updated by author(s): Jun 1, 2021

# Reporting Summary

Nature Research wishes to improve the reproducibility of the work that we publish. This form provides structure for consistency and transparency in reporting. For further information on Nature Research policies, see Authors & Referees and the Editorial Policy Checklist.

## Statistics

For all statistical analyses, confirm that the following items are present in the figure legend, table legend, main text, or Methods section.

| n/a | Confirmed | |
|---|---|---|
| ☐ | ☒ | The exact sample size (*n*) for each experimental group/condition, given as a discrete number and unit of measurement |
| ☐ | ☒ | A statement on whether measurements were taken from distinct samples or whether the same sample was measured repeatedly |
| ☐ | ☒ | The statistical test(s) used AND whether they are one- or two-sided<br>*Only common tests should be described solely by name; describe more complex techniques in the Methods section.* |
| ☐ | ☒ | A description of all covariates tested |
| ☐ | ☒ | A description of any assumptions or corrections, such as tests of normality and adjustment for multiple comparisons |
| ☐ | ☒ | A full description of the statistical parameters including central tendency (e.g. means) or other basic estimates (e.g. regression coefficient) AND variation (e.g. standard deviation) or associated estimates of uncertainty (e.g. confidence intervals) |
| ☐ | ☒ | For null hypothesis testing, the test statistic (e.g. *F*, *t*, *r*) with confidence intervals, effect sizes, degrees of freedom and *P* value noted<br>*Give P values as exact values whenever suitable.* |
| ☒ | ☐ | For Bayesian analysis, information on the choice of priors and Markov chain Monte Carlo settings |
| ☒ | ☐ | For hierarchical and complex designs, identification of the appropriate level for tests and full reporting of outcomes |
| ☐ | ☒ | Estimates of effect sizes (e.g. Cohen's *d*, Pearson's *r*), indicating how they were calculated |

*Our web collection on statistics for biologists contains articles on many of the points above.*

## Software and code

Policy information about availability of computer code

| | |
|---|---|
| Data collection | Images of agarose gel were collected by Bio-Rad Image Lab™ software or MP1600 Tanon imaging software.<br>The qPCR data was acquired by QuantStudio™ Software V1.3 on Applied Biosystems ViiATM7 Real-Time PCR System (Applied Biosystems, USA).<br>The western blot data was acquired by MP-5200 Tanon imaging software on a 5200 chemiluminescence imaging machine (Tanon, China).<br>The sections stained with Safranin O (Coolaber, China) and Fast Green (Coolaber, China) was imaged by cellSens Standard 1.9 Olympus imaging software under bright-field through a microscope (Olympus, IX73, Japan).<br>Tiller buds at shoot basal regions of 4-leaf stage seedlings were imaged by NIS Elements 4.60 Nikon imaging software under bright-field through a microscope (Nikon, SMZ 18, Japan).<br>Root morphological parameters were collected by EPSON scanner (Epson Expression 1600pro, Japan) and Win-RHZIO software (Regent Instruments Inc., Canada).<br>Photosynthesis datas were collected by LI-6800 (LI-COR Inc., USA).<br>The fluorescence images were taken immediately using ZEN lite from a Zeiss LSM 700 laser scanning confocal microscope (Germany).<br>Mass spectrometry data was collected by Agilent MassHunter Workstation Software in a Triple Quad 5500 mass spectrometer (AB SCIEX, USA).<br>Poly(A) RNA quantification data was collected by Agilent bioanalyzer 2100 (USA).<br>Ploidy data was acquired by BD LSRFortessa cell analyzer (USA)<br>High through-put sequencing data was collected by illumina HiSeq Control Software v3.4.0 for HiSeq 4000 Systems. |
| Data analysis | Cutadapt v1.15 was used to trim adapters of raw reads.<br>HISAT2 v2.1.0 was used to map reads to the rice genome.<br>MeTPeak was used to identify m6A peaks.<br>HOMER v4.9 was used for motif enrichment analysis.<br>featureCounts from Subread v1.6.4 was used for counting reads.<br>The R package affy was used for normalizing gene expression.<br>agriGO v2.0 was used to perform GO analysis. |

Flow cytometry data was collected with BD FACSDiva 7.0, analyzed and exported by flowJo10.5.3.
The GSEA software was used for gene set enrichment analysis.
EnrichmentMap was used to show the GSEA network.

For manuscripts utilizing custom algorithms or software that are central to the research but not yet described in published literature, software must be made available to editors/reviewers. We strongly encourage code deposition in a community repository (e.g. GitHub). See the Nature Research guidelines for submitting code & software for further information.

## Data

Policy information about availability of data

All manuscripts must include a data availability statement. This statement should provide the following information, where applicable:

- Accession codes, unique identifiers, or web links for publicly available datasets
- A list of figures that have associated raw data
- A description of any restrictions on data availability

The m6A-seq and quantitative RNA-seq data generated by this study have been deposited in NCBI Gene Expression Omnibus (GEO) under the accession number GSE135549. All other data supporting the findings of this study are available from the corresponding authors on reasonable request.

# Field-specific reporting

Please select the one below that is the best fit for your research. If you are not sure, read the appropriate sections before making your selection.

☒ Life sciences ☐ Behavioural & social sciences ☐ Ecological, evolutionary & environmental sciences

For a reference copy of the document with all sections, see nature.com/documents/nr-reporting-summary-flat.pdf

# Life sciences study design

All studies must disclose on these points even when the disclosure is negative.

| | |
|---|---|
| Sample size | Sample sizes were determined based on the Authors' experience of what is necessary to generate a convincing and compelling result. The sample size (n) of each experiment is provided in the figure/table legends in the main manuscript and supplementary information files. For laboratory and greenhouse experiments: in our laboratory, we regularly use at least 3 biological replicates (with exceptions for the seq data) which results in reproducible data and the detection of significant changes that support meaningful conclusions. For the field trial: there were 32 plants for each rice genotype in one plot and each genotype was arranged in 3 random plots, as this amount of replication is adequate to detect meaningful (biologically and practically) phenotypic changes in rice; there were more than 100 plants for each genotype of potato in one plots and each genotype was grown in 3 random plots. |
| Data exclusions | No data points were excluded from analysis in any experiment depicted in this manuscript. |
| Replication | The findings in this paper were remarkably reproducible. Every experiment was performed multiple times. |
| Randomization | All crops included in this paper were grown in the fields in a random arrangement. |
| Blinding | The investigators were blinded to genotypes during phenotype associated data collection, especially yield data collection. |

# Reporting for specific materials, systems and methods

We require information from authors about some types of materials, experimental systems and methods used in many studies. Here, indicate whether each material, system or method listed is relevant to your study. If you are not sure if a list item applies to your research, read the appropriate section before selecting a response.

### Materials & experimental systems

| n/a | Involved in the study |
|---|---|
| ☐ | ☒ Antibodies |
| ☒ | ☐ Eukaryotic cell lines |
| ☒ | ☐ Palaeontology |
| ☒ | ☐ Animals and other organisms |
| ☒ | ☐ Human research participants |
| ☒ | ☐ Clinical data |

### Methods

| n/a | Involved in the study |
|---|---|
| ☒ | ☐ ChIP-seq |
| ☐ | ☒ Flow cytometry |
| ☒ | ☐ MRI-based neuroimaging |

## Antibodies

| | |
|---|---|
| Antibodies used | The primary antibodies used were commercially available: mouse anti-FTO antibody (ab92821, Abcam, USA), rabbit anti-Histone |

| | |
|---|---|
| | H3 antibody (ab1791, Abcam, USA), mouse anti-H3K9me2 antibody (ab1220, Abcam, USA ), and anti-H3K27me3 antibody (61017, Active motif, USA), and mouse anti-β-actin (HX1843, Huaxingbio Biotechnology, China). |
| Validation | Further information on these antibodies is available at https://www.abcam.com/, https://www.activemotif.com/, and http://www.huaxingbio.com/. |

## Flow Cytometry

### Plots

Confirm that:

☒ The axis labels state the marker and fluorochrome used (e.g. CD4-FITC).

☒ The axis scales are clearly visible. Include numbers along axes only for bottom left plot of group (a 'group' is an analysis of identical markers).

☐ All plots are contour plots with outliers or pseudocolor plots.

☐ A numerical value for number of cells or percentage (with statistics) is provided.

### Methodology

| | |
|---|---|
| Sample preparation | To examine the ploidy level of FTO plants in this analysis, fresh leaves were chopped with a sharp razor in precooled extraction buffer (0.1M citric acid, 0.5% Tween 20, pH 2.3). After filtered through 30 μm cell strainer, the DNA content per nucleus stained with DAPI were measured by using the BD LSRFortessaTM cell analyzer (USA). |
| Instrument | BD LSRFortessa cell analyzer (USA) |
| Software | Flow cytometry data was collected with BD FACSDiva 7.0, analyzed and exported by flowJo10.5.3 |
| Cell population abundance | No sorting was done, just analysis the data according to gating strategy. |
| Gating strategy | Nuclei for analysis was gated according to the FSC and SSC channel.To reduce interference from debris and other cellular particles, events were gated on SSC and DAPI fluorescence to distinguish between noise and fluorescence signals from the nucleus. |

☒ Tick this box to confirm that a figure exemplifying the gating strategy is provided in the Supplementary Information.